A&A 466, 763–770 (2007)
DOI: 10.1051/0004-6361:20066782

Astronomy & Astrophysics

Atomic data from the IRON project⋆

LXIII. Electron-impact excitation of Fe^{19+} up to $n = 4$

M. C. Witthoeft[1], G. Del Zanna[2], and N. R. Badnell[1]

[1] Department of Physics, University of Strathclyde, Glasgow, G4 0NG, UK
e-mail: witthoef@phys.strath.ac.uk
[2] MSSL, University College London, Holmbury St., Mary Dorking, RH5 6NT, UK

Received 21 November 2006 / Accepted 1 February 2007

ABSTRACT

We present results for the electron-impact excitation of N-like Fe as part of the RmaX network. *R*-matrix theory using an intermediate-coupling frame transformation method is used to obtain level-resolved collision strengths. Separate calculations are performed using different target expansions. The first is a 215 level close-coupling calculation which has the $2s^2\ 2p^3$, $2s\ 2p^4$, $2p^5$, $2s^2\ 2p^2\ 3l$, and $2s\ 2p^3\ 3l$ configurations while the second calculation also includes the levels from the $2s^2\ 2p^2\ 4l$ configurations for a total of 302 close-coupling levels. The effect of the additional resonant enhancement of the larger calculation is explored and compared with a previous IRON Project report and other, more recent, calculations. As a final comparison, we model an astrophysical plasma using the results of the present calculations and previous work.

Key words. atomic data – atomic processes – scattering

1. Introduction

The purpose of the IRON Project (Hummer et al. 1993) is to perform large-scale electron-scattering calculations for ions of astophysical importance. The RmaX[1] network within the IRON Project is aimed at providing collisional data for transitions at X-ray wavelengths. The current work, as a part of the RmaX effort, extends the previous IRON Project calculation (IP XLIX) on N-like Fe by Butler & Zeippen (2001). This older work was an 86 level Breit-Pauli *R*-matrix calculation which included the $2s^2\ 2p^3$, $2s\ 2p^4$, $2p^5$, $2s^2\ 2p^2\ 3l$, and select $2s\ 2p^3\ 3l$ levels. Originally, the goal of this work was to extend these calculations to include transitions to all $2s\ 2p^3\ 3l$ and $2s^2\ 2p^2\ 4l$ levels using the intermediate-coupling frame transformation (ICFT) method. This is thought necessary because we have found in other cases (e.g. Fe^{17+}; Witthoeft et al. 2005) that the inclusion of $n = 4$ levels changed the ion population considerably. However, this work also corrects an error found in the Butler & Zeippen work, which will be discussed in detail later.

Besides the previous IRON Project calculation, McLaughlin & Kirby (2001) performed a 23-level Breit-Pauli *R*-matrix calculation primarily focused on transitions between the $2s^2\ 2p^3$, $2s\ 2p^4$, and $2p^5$ levels. The effective collision strengths for these transitions are currently included in the CHIANTI v. 5 database. Most recently, a large distorted wave calculation to $n = 5$ was carried out by Landi & Gu (2006) where resonance effects were included for configurations with $n \leq 3$. Their work was aimed at providing accurate effective collision strengths at higher temperatures and is also included in the current version of the CHIANTI database (v. 5; Landi et al. 2006).

The Fe^{19+} system produces a large number of spectral lines observed from the X-rays to the UV. A considerable number of $2s^2\ 2p^3 - 2s^2\ 2p^2\ 3d$ transitions are observed in the X-rays, in particular at high densities (laser spectra), but also in astrophysical spectra (solar flares, active stars). The $2s^2\ 2p^3 - 2s\ 2p^4$ transitions are prominent in EUV spectra of solar flares (e.g. Kastner et al. 1974), active stars and Tokamaks (e.g. Stratton et al. 1984), and can be used to measure electron densities. The forbidden $2s^2\ 2p^3$ transitions show up as prominent lines in the UV (cf. Kucera et al. 2000).

The rest of the paper is organized as follows. In Sect. 2, we outline the calculation details and perform structure comparisons with the results of other calculations and measurements. Analysis of the effective collision strengths with previous calculations is performed in Sect. 3 along with a look at level populations and line intensities. Finally, we summarize our results in Sect. 4.

2. Calculation and structure

The present work consists of two *R*-matrix calculations. The first, referred to hereafter as the $3l$ calculation, contains the following configurations: $2s^2\ 2p^3$, $2s\ 2p^4$, $2p^5$, $2s^2\ 2p^2\ 3l$, and $2s\ 2p^3\ 3l$ with $l = 0, 1, 2$. The second calculation, we will call $4l$, extends the $3l$ target expansion by including the $2s^2\ 2p^2\ 4l$ configurations with $l = 0{-}3$. The smaller calculation has 120 LS terms and 215 fine-structure levels while the $4l$ calculation has 284 terms and 302 levels. The structure of each calculation was determined using AUTOSTRUCTURE (Badnell 1986) where radial scaling parameters were used to

⋆ The full list of energy levels (Table 2) is available in electronic form at the CDS via anonymous ftp to
cdsarc.u-strasbg.fr (130.79.128.5) or via
http://cdsweb.u-strasbg.fr/cgi-bin/qcat?J/A+A/466/763

[1] Web page: http://amdpp.phys.strath.ac.uk/UK_RmaX/

Table 1. Radial scaling parameters used in AUTOSTRUCTURE.

	$n = 3$	$n = 4$
λ_{1s}	1.4112	1.4149
λ_{2s}	1.3257	1.3452
λ_{2p}	1.2550	1.2709
λ_{3s}	1.2388	1.2307
λ_{3p}	1.1850	1.1772
λ_{3d}	1.2619	1.2466
λ_{4s}	–	1.2308
λ_{4p}	–	1.1814
λ_{4d}	–	1.2425
λ_{4f}	–	1.2870

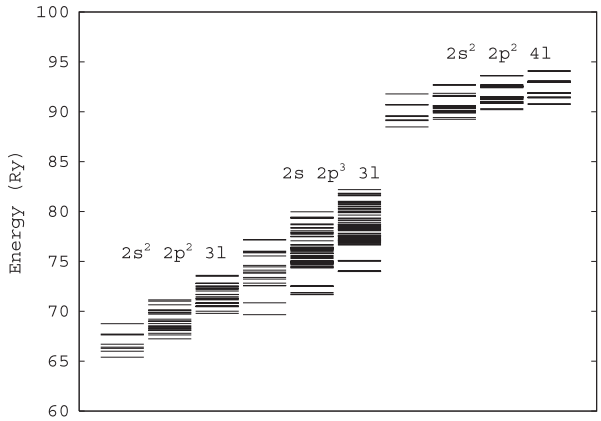

Fig. 1. Energy levels in Ry from the $4l$ calculation from AUTOSTRUCTURE. For each nl-configuration, the levels are further split by the angular momentum of the valence electron, increasing from left-to-right.

minimize the equally-weighted sum of all LS term energies in the Thomas-Fermi approximation. These scaling parameters are given in Table 1 for both calculations.

The energy levels for the $4l$ calculation are shown in Fig. 1, split by configuration. Within each nl-configuration, the levels are further split, increasing from left-to-right, by the angular momentum of the valence electron. There is a lot of overlap between the $2s^2\ 2p^2\ 3l$ and $2s\ 2p^3\ 3l$ levels but the $2s^2\ 2p^2\ 4l$ levels are well separated from the rest. Due to the overlap of the $n = 3$ levels, the configuration and term of each level are not reliable labels for identification. When comparing the collision strengths from different calculations it is important to identify the levels by only the total angular momentum, parity, and energy order while ignoring the configuration and term labels.

In Table 2 are listed the $4l$ level energies for the $2s^2\ 2p^3$, $2s\ 2p^4$, $2p^5$, and $2s^2\ 2p^2\ 3l$ configurations, together with those from NIST v. 3. As the $3l$ energies agree well with the $4l$ energies, they are not included in the table. For the $2l^5$ levels, we find good agreement with the NIST values, as well as those from previous calculations by Butler & Zeippen (2001) and McLaughlin & Kirby (2001). The energies of the recent distorted wave calculation of Landi & Gu (2006) show better agreement with observations for these levels, presumably because of the larger target expansion (they include 725 levels). A comparison of level energies in the higher configurations is shown in Fig. 2. Here, we plot the percentage difference of the present $3l$ calculation energies, observed energies listed in CHIANTI v. 5 and NIST, and the energies of Landi & Gu (2006), with the present $4l$ calculation. As previously mentioned, there is very good agreement between the energies of the present $3l$ and $4l$ calculations. However, the additional $n = 4$ configurations lead to a slight improvement of the $4l$ energies compared to the $3l$ calculation for these higher levels. Generally speaking, the energies of the $4l$ calculation are between 0.2 and 0.4% higher than the observed energies. For the $2s^2\ 2p^2\ 4l$ levels, the agreement between the $4l$ calculation energies and the NIST energies is worse, but still under 1%. The agreement between the energies of the present calculation and those of Landi & Gu is also between 0.2 and 0.4% for the higher levels. The Landi & Gu energies are in better agreement with the observed energies for most of these levels. Overall, the energy differences seen between the calculations are small and in good agreement with observations. While the location of spectral features are shifted due to these differences, the overall magnitude of the collision strengths should not be affected since the energy-order of the levels is correct with few exceptions. Also, due to the fact that these energy differences are small, we expect that the level mixing is accurate.

It is also useful to check oscillator strengths and A-values to get a better idea of the accuracy of our structure. In Table 3, the gf-values of the $3l$ and $4l$ calculations for transitions from the ground level to the $2s^2\ 2p^2\ 3s/3d$ levels are compared with the Case B calculation of Mason & Bhatia (1983). Generally, we see good agreement between the calculations for all transitions with few exceptions, in particular the transitions to the higher levels. In Table 5, we include A-value comparisons for the strongest transitions and find excellent agreement with NIST and a recent calculation of Jonauskas et al. (2005). We do find, however, large differences with some transitions (including some very strong transitions) of our A-values and those of a previous IRON Project report by Nahar (2004). This will be further discussed in Sect. 3.2.

The scattering calculations were performed using the intermediate-coupling frame transformation (ICFT) method (see Griffin et al. 1998) which employs multi-channel quantum defect theory (MQDT) to obtain level-resolved collision strengths from a term-resolved R-matrix calculation. Both calculations include the mass-velocity, spin-orbit, and Darwin relativistic corrections. The $3l$ and $4l$ calculations use 20 and 30 continuum basis functions respectively. In the R-matrix inner region, exchange effects were included for $J = 0{-}10$ for the $3l$ calculation and $J = 0{-}12$ for the $4l$ calculation. This range is extended to $J = 40$ for both calculations using a non-exchange approximation. A further top-up of the collision strengths to infinite J was added using the Burgess sum rule (see Burgess 1974) for dipole transitions and a geometric series for the non-dipole transitions (see Badnell & Griffin 2001). In the outer region, an energy mesh of $10^{-5}\ z^2$ Ry (where $z = 19$ for N-like Fe) was used in the resonance region of the exchange calculation. A mesh of $10^{-3}\ z^2$ Ry was used beyond the resonance region of the exchange calculation and over the entire energy range of the non-exchange calculation up to an energy of 420 Ry, or near 3.5 times the ionization threshold. The fine energy mesh used in the resonance region is not small enough to fully resolve all of the resonances, however, as discussed by Badnell & Griffin (2001), this mesh is small enough to accurately sample the small width resonances. Effective collision strengths are then obtained by convoluting the collision strengths with a Maxwellian distribution, where interpolation to infinite-energy limit points is used to calculate the effective collision strengths beyond our calculated energy range. The infinite-energy collision strengths are calculated for dipole and allowed transitions within AUTOSTRUCTURE (see Whiteford et al. 2001).

Table 2. Energy levels of the $2s^2\ 2p^3$, $2s\ 2p^4$, $2p^5$, and $2s^2\ 2p^2\ 3l$ configurations for the present $4l$ calculation, compared to NIST (v. 3). For the $2s^2\ 2p^2\ 3l$ levels, we use only the valence electron as a label to save space. Gaps in the level-index sequence indicate the presence of a level from another configuration. All energies are given in Ry. (Full table available at the CDS.)

idx	conf	$4l$	NIST	idx	conf	$4l$	NIST	idx	conf	$4l$	NIST
1	$2s^2\ 2p^3\ ^4S^o_{3/2}$	0.000	0.000	25	$3p\ ^2S^o_{1/2}$	67.798	–	50	$3d\ ^4D_{3/2}$	70.779	–
2	$2s^2\ 2p^3\ ^2D^o_{3/2}$	1.294	1.263	26	$3p\ ^4P^o_{3/2}$	68.074	–	51	$3d\ ^4D_{7/2}$	70.809	–
3	$2s^2\ 2p^3\ ^2D^o_{5/2}$	1.674	1.605	27	$3p\ ^4D^o_{5/2}$	68.150	–	52	$3d\ ^2F_{5/2}$	70.824	–
4	$2s^2\ 2p^3\ ^2P^o_{1/2}$	2.411	2.372	28	$3p\ ^4P^o_{1/2}$	68.266	–	53	$3d\ ^4F_{9/2}$	70.839	–
5	$2s^2\ 2p^3\ ^2P^o_{3/2}$	3.005	2.946	29	$3p\ ^4P^o_{5/2}$	68.352	–	55	$3p\ ^2P^o_{1/2}$	71.016	–
6	$2s\ 2p^4\ ^4P_{5/2}$	6.906	6.859	30	$3p\ ^2D^o_{3/2}$	68.453	–	56	$3d\ ^4P_{5/2}$	71.142	71.097
7	$2s\ 2p^4\ ^4P_{3/2}$	7.519	7.478	31	$3p\ ^4D^o_{7/2}$	68.551	–	57	$3p\ ^2P^o_{3/2}$	71.143	–
8	$2s\ 2p^4\ ^4P_{1/2}$	7.720	7.677	32	$3s\ ^2S_{1/2}$	68.762	–	58	$3d\ ^4P_{3/2}$	71.248	71.097
9	$2s\ 2p^4\ ^2D_{3/2}$	9.615	9.501	33	$3p\ ^4S^o_{3/2}$	68.764	–	59	$3d\ ^2P_{1/2}$	71.267	–
10	$2s\ 2p^4\ ^2D_{5/2}$	9.780	9.644	34	$3p\ ^2P^o_{3/2}$	68.992	–	60	$3d\ ^4P_{1/2}$	71.329	–
11	$2s\ 2p^4\ ^2S_{1/2}$	11.014	10.892	35	$3p\ ^2D^o_{5/2}$	69.037	–	61	$3d\ ^2F_{7/2}$	71.455	71.261
12	$2s\ 2p^4\ ^2P_{3/2}$	11.475	11.322	36	$3p\ ^2P^o_{1/2}$	69.213	–	63	$3d\ ^2D_{3/2}$	71.675	71.616
13	$2s\ 2p^4\ ^2P_{1/2}$	12.371	12.211	38	$3p\ ^2F^o_{5/2}$	69.710	–	64	$3d\ ^2D_{5/2}$	71.690	71.471
14	$2p^5\ ^2P^o_{3/2}$	18.030	17.809	39	$3d\ ^4F_{3/2}$	69.791	–	67	$3d\ ^2G_{7/2}$	72.028	–
15	$2p^5\ ^2P^o_{1/2}$	19.037	18.790	40	$3p\ ^2F^o_{7/2}$	69.833	–	68	$3d\ ^2G_{9/2}$	72.179	–
16	$3s\ ^4P_{1/2}$	65.403	–	41	$3p\ ^2D^o_{3/2}$	69.910	–	69	$3d\ ^2D_{3/2}$	72.300	72.163
17	$3s\ ^4P_{3/2}$	65.996	–	42	$3d\ ^4F_{5/2}$	70.010	–	70	$3d\ ^2D_{5/2}$	72.346	72.109
18	$3s\ ^2P_{1/2}$	66.288	–	43	$3p\ ^2D^o_{5/2}$	70.086	–	71	$3d\ ^2P_{1/2}$	72.483	–
19	$3s\ ^4P_{5/2}$	66.402	–	44	$3p\ ^2P^o_{1/2}$	70.150	–	74	$3d\ ^2F_{7/2}$	72.552	72.309
20	$3s\ ^2P_{3/2}$	66.704	–	45	$3d\ ^2P_{3/2}$	70.458	–	79	$3d\ ^2S_{1/2}$	72.798	–
21	$3p\ ^4D_{1/2}$	67.236	–	46	$3d\ ^4F_{7/2}$	70.474	–	80	$3d\ ^2P_{3/2}$	72.808	72.601
22	$3p\ ^4D_{3/2}$	67.629	–	47	$3d\ ^4D_{1/2}$	70.521	–	81	$3d\ ^2F_{5/2}$	72.813	72.746
23	$3s\ ^2D_{5/2}$	67.629	–	48	$3d\ ^4D_{5/2}$	70.550	–	85	$3d\ ^2D_{5/2}$	73.507	73.330
24	$3s\ ^2D_{3/2}$	67.721	–	49	$3p\ ^2P^o_{3/2}$	70.655	–	86	$3d\ ^2D_{3/2}$	73.602	–

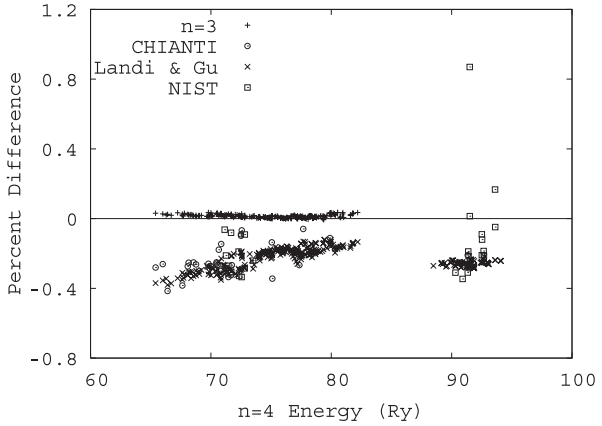

Fig. 2. Percent difference of the $3l$ and Landi & Gu (2006) calculations, and the observed energies from NIST and CHIANTI v. 5, with the present $4l$ calculation.

3. Results

3.1. Comparison of effective collision strengths

The primary purpose of this work is to improve on the previous IRON Project calculation by Butler & Zeippen (2001), following the findings of our previous work on Fe^{17+} (Witthoeft et al. 2006). However, errors have been found in the high-energy collision strengths of some transitions calculated by Butler & Zeippen, where large "jumps" in the collision strength can be seen just beyond the resonance region. These discontinuous "jumps" are caused by the incorrect matching of the levels of the low-energy collision strengths with those of the high-energy collision strengths (Butler 2005). An example of this is shown in Fig. 3, along with the collision strengths for the two present calculations. For these transitions, the high temperature effective collisions strengths will be unphysically enhanced (or suppressed in the case of "drops" in the collision strength) in the Butler & Zeippen calculation. We also show, in Fig. 5, the effect of these "jumps" on the effective collision strength for the same transition shown in Fig. 3. Between the two present calculations, we see that the $4l$ resonances extend to much larger energy than the $3l$ calculation. However, note that we are plotting the logarithm of the collision strength, so the magnitude of these extra resonances is actually small compared to the $3l$ resonances and will have a small effect on the effective collision strength for this transition. The differences between the two present calculations at low temperatures is primarily due to differences in the $n = 3$ resonance structure.

In light of the errors in the Butler & Zeippen calculation, our primary comparison will be with those data currently included in the CHIANTI v. 5 database. For transitions between the $2s^2\ 2p^3$, $2s\ 2p^4$, and $2p^5$ levels, we will compare with the 23-level Breit-Pauli R-matrix calculation of McLaughlin & Kirby (2001). For transitions to the higher levels we will compare with the recent distorted wave calculation (up to $n = 5$) of Landi & Gu (2006), where the approximate effects of the $n \leq 3$ resonances have been included. Comparisons are made at the peak abundance temperature for photo-ionized plasmas, $T \approx 4 \times 10^5$ K (Kallman & Bautista 2001), and collision-dominated plasmas, $T \approx 1 \times 10^7$ K (Mazzotta et al. 1998).

In Table 4, we compare the effective collision strengths of the $3l$ and $4l$ calculations with the Breit-Pauli R-matrix calculation of McLaughlin & Kirby (2001). There is generally very good agreement between the $3l$ and $4l$ calculations at both temperatures. Interestingly, the agreement is slightly better for most

Table 3. Comparison of gf-values of the present calculations with the Case B calculation of Mason & Bhatia (1983) for transitions to $2s^2\ 2p^2\ 3s/3d$ levels from the ground level. The indices, i and j, are the energy-ordered level indices of the $4l$ calculation.

i	j	j level	$4l$	$3l$	Mason & Bhatia
1	16	$2s^2\ 2p^2\ 3s\ ^4P_{1/2}$	7.610E-02	7.433E-02	6.768E-02
1	17	$2s^2\ 2p^2\ 3s\ ^4P_{3/2}$	1.221E-01	1.177E-01	1.157E-01
1	18	$2s^2\ 2p^2\ 3s\ ^2P_{1/2}$	4.978E-05	3.703E-05	4.511E-05
1	19	$2s^2\ 2p^2\ 3s\ ^4P_{5/2}$	1.843E-01	1.763E-01	1.809E-01
1	20	$2s^2\ 2p^2\ 3s\ ^2P_{3/2}$	1.602E-03	1.433E-03	1.506E-03
1	23	$2s^2\ 2p^2\ 3s\ ^2D_{5/2}$	5.793E-03	5.458E-03	6.375E-03
1	24	$2s^2\ 2p^2\ 3s\ ^2D_{3/2}$	8.727E-04	8.536E-04	1.041E-03
1	32	$2s^2\ 2p^2\ 3s\ ^2S_{1/2}$	2.228E-05	2.535E-05	2.060E-05
1	39	$2s^2\ 2p^2\ 3d\ ^4F_{3/2}$	7.624E-02	7.665E-02	6.978E-02
1	42	$2s^2\ 2p^2\ 3d\ ^4F_{5/2}$	3.999E-01	4.043E-01	3.844E-01
1	45	$2s^2\ 2p^2\ 3d\ ^2P_{3/2}$	2.207E-01	2.178E-01	2.100E-01
1	47	$2s^2\ 2p^2\ 3d\ ^4D_{1/2}$	3.231E-02	3.234E-02	3.076E-02
1	48	$2s^2\ 2p^2\ 3d\ ^4D_{5/2}$	5.085E-01	5.166E-01	5.008E-01
1	50	$2s^2\ 2p^2\ 3d\ ^4D_{3/2}$	5.139E-02	5.276E-02	5.188E-02
1	52	$2s^2\ 2p^2\ 3d\ ^2F_{5/2}$	7.316E-01	7.225E-01	6.980E-01
1	56	$2s^2\ 2p^2\ 3d\ ^4P_{5/2}$	1.969E+00	1.947E+00	2.043E+00
1	58	$2s^2\ 2p^2\ 3d\ ^4P_{3/2}$	1.997E+00	1.981E+00	2.031E+00
1	59	$2s^2\ 2p^2\ 3d\ ^2P_{1/2}$	2.175E-01	2.161E-01	1.926E-01
1	60	$2s^2\ 2p^2\ 3d\ ^4P_{1/2}$	9.142E-01	9.059E-01	9.521E-01
1	63	$2s^2\ 2p^2\ 3d\ ^2D_{3/2}$	1.696E-02	2.152E-02	2.052E-02
1	64	$2s^2\ 2p^2\ 3d\ ^2D_{5/2}$	2.128E-01	2.160E-01	1.690E-01
1	69	$2s^2\ 2p^2\ 3d\ ^2D_{3/2}$	1.897E-02	1.891E-02	1.223E-02
1	70	$2s^2\ 2p^2\ 3d\ ^2D_{5/2}$	1.012E-02	7.927E-03	1.698E-02
1	71	$2s^2\ 2p^2\ 3d\ ^2P_{1/2}$	1.146E-02	1.109E-02	1.124E-03
1	79	$2s^2\ 2p^2\ 3d\ ^2S_{1/2}$	1.138E-02	1.148E-02	1.129E-02
1	80	$2s^2\ 2p^2\ 3d\ ^2P_{3/2}$	1.080E-02	1.036E-02	9.000E-03
1	81	$2s^2\ 2p^2\ 3d\ ^2F_{5/2}$	1.872E-02	1.769E-02	4.929E-03
1	85	$2s^2\ 2p^2\ 3d\ ^2D_{5/2}$	8.887E-04	1.027E-03	1.789E-03
1	86	$2s^2\ 2p^2\ 3d\ ^2D_{3/2}$	7.473E-06	2.701E-06	3.257E-05

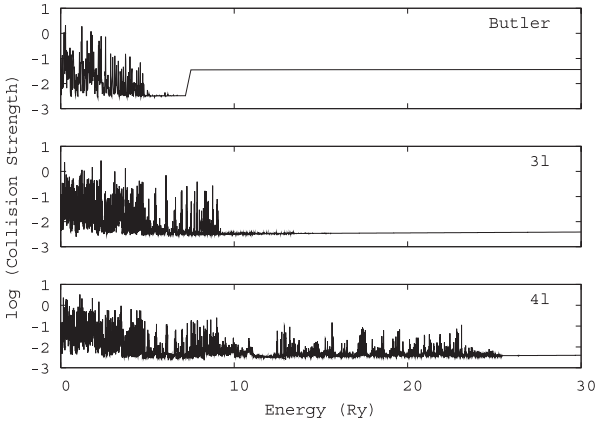

Fig. 3. Collision strength for the transition to $2s^2\ 2p^2\ 3s\ ^4P_{5/2}$ from the ground level. From top to bottom, the results shown are from Butler & Zeippen (2001), the $3l$ calculation, and the $4l$ calculation.

transitions at the high temperature, despite the extra resonant enhancement present in the $4l$ calculation. This is most likely due to the fact that the background of the $3l$ calculation is slightly higher than the $4l$ calculation for all but two of these transitions. The agreement between the present calculations and those of McLaughlin & Kirby are at the 30% level (on average) for the lower temperature and the 15% level for the high temperature. The background collision strengths at high energies between McLaughlin & Kirby's calculation and our own is in good agreement, so the differences in the Table 4 are most likely due to resonance effects. We would expect there to be better agreement between McLaughlin & Kirby and our $3l$ calculation, since they included only the $2s^2\ 2p^3$, $2s\ 2p^4$, $2p^5$, and $2s^2\ 2p^2\ 3l$ configurations in their calculation, but this is not always the case. The most probable reason for the difference is due to the resonance resolution of the two calculations. In the McLaughlin & Kirby calculation, an energy mesh of $10^{-4}\ z^2$ Ry was used in the resonance region whereas a mesh of $10^{-5}\ z^2$ Ry is used in the present work. This is confirmed by the better agreement between the calculations at the higher temperature where the resonance contribution to the effective collision strength is smaller.

Next we will look at the transitions to the $2s^2\ 2p^2\ 3l$ levels from the ground level. At near the peak abundance temperature for collision-dominated plasmas ($T = 1.2 \times 10^7$ K), the agreement between the present results and those of the recent distorted wave calculation by Landi & Gu (2006) agree at the 10% level for the strongest transitions. For several of the weaker transitions, however, we find that the present calculations give results more than a factor of two greater than the distorted wave calculation. Landi & Gu provide effective collision strengths down to a temperature of 1.1×10^6 K, where we find that the differences between the calculations are larger overall. This is probably due to the approximate treatment of the resonances in the distorted wave calculations. We note that the collision strengths used by Landi & Gu were calculated by Gu (2003) for a temperature range between 3.17×10^6 and 3.55×10^7 K. These resonant enhanced collision strengths were extrapolated to the lower temperatures given in Landi & Gu. In Fig. 4, we compare the $4l$ calculation with the results of Landi & Gu at a temperature of $4{\times}10^6$ K by plotting the ratio of the $4l$ effective collision strength to that of Landi & Gu versus the magnitude of the $4l$ collision

Table 4. Effective collision strengths of the present 3*l* and 4*l* calculations compared with those of McLaughlin & Kirby (2001) (denoted as M&K). Values are given at the peak abundance temperatures for Fe^{19+} in photo-ionized plasmas and collision-dominated plasmas.

	$T = 4 \times 10^5$ K			$T = 1.2 \times 10^7$ K		
i-j	3*l*	4*l*	M&K	3*l*	4*l*	M&K
1-2	1.10E-1	1.19E-1	9.08E-2	5.11E-2	5.04E-2	4.59E-2
1-3	7.53E-2	8.35E-2	6.31E-2	5.05E-2	4.80E-2	4.63E-2
1-4	2.34E-2	2.32E-2	1.76E-2	1.72E-2	1.51E-2	1.47E-2
1-5	3.81E-2	4.25E-2	3.71E-2	2.63E-2	2.65E-2	2.20E-2
2-3	1.14E-1	1.15E-1	8.92E-2	8.40E-2	8.81E-2	6.59E-2
2-4	9.90E-2	9.79E-2	5.27E-2	3.95E-2	3.95E-2	3.80E-2
2-5	9.25E-2	9.22E-2	4.58E-2	5.20E-2	5.38E-2	4.06E-2
3-4	5.11E-2	5.12E-2	3.40E-2	3.35E-2	3.14E-2	3.19E-2
3-5	2.02E-1	1.87E-1	1.02E-1	9.60E-2	9.35E-2	8.40E-2
4-5	4.89E-2	4.70E-2	3.60E-2	3.82E-2	4.08E-2	2.94E-2

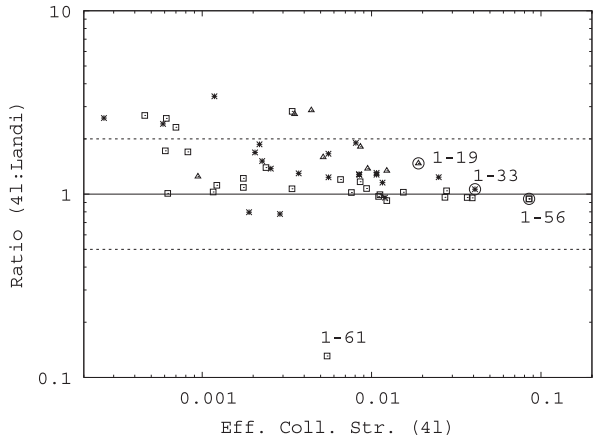

Fig. 4. The ratio of the effective collision strengths of the present 4*l* calculation to the Landi & Gu results at a temperature of 4×10^6 K. Only transitions between the ground level and the levels belonging to the $2s^2\ 2p^2\ 3l$ configurations are plotted. The triangles show transitions to the 3s levels, the stars are 3p levels, and the boxes are the 3d levels. The dotted curves mark differences of a factor of two. The strongest transition to each configuration has been circled and labeled according to the energy-ordered index of the 4*l* calculation for further discussion.

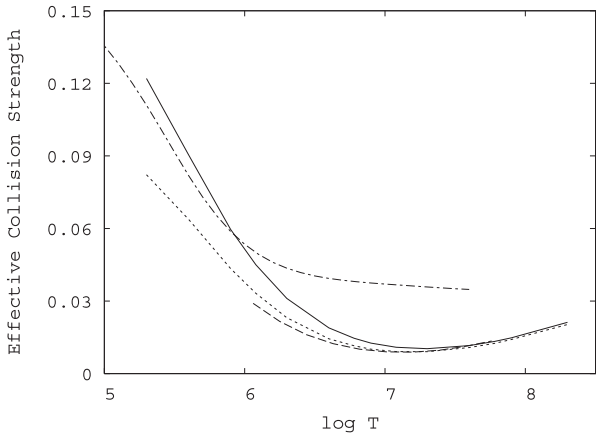

Fig. 5. Effective collision strength for the transition to $2s^2\ 2p^2\ 3s\ ^4P_{5/2}$ from the ground level (1−19). The solid and dotted curves are the 4*l* and 3*l* calculations, respectively. The dashed curve is the result from Landi & Gu (2006) and the dot-dashed curve is the result of Butler & Zeippen (2001).

strength. We show only the ratios for the transitions between the ground level and the $2s^2\ 2p^2\ 3l$ levels in the figure; triangles denote 3s transitions, stars are for 3p transitions, and the boxes mark the 3d transitions. The agreement with the stronger transitions to the $2s^2\ 2p^2$ 3d levels is still quite good, but the 4*l* calculations give consistantly larger results for the transitions to the $2s^2\ 2p^2$ 3s and $2s^2\ 2p^2$ 3p levels. The strongest transition to each configuration has been circled and labeled according to the energy-ordered index of the 4*l* calculation (see Table 2). To assess the accuracy of the isolated-resonance approximation used in the collision strengths of Landi & Gu, it is more proper to look at ratios between the present 3*l* calculation and the results of Landi & Gu since only resonances up to $n = 3$ were included in their calculations. For transitions to the 3d levels, which do not show much resonant enhancement, such a comparison yields similar results to what is seen in Fig. 4 (approximately 65% of the transitions agree within 20% in both cases). However, for transitions to the 3s and 3p levels, there is improved agreement of the Landi & Gu results with the present 3*l* calculation rather than the 4*l* calculation. While only 10% of these transitions agree within 20% in the 4*l* comparison, half of these transitions agree within 20% when comparing the Landi & Gu results with the 3*l* results.

In Fig. 5 is shown the effective collision strength for the 1−19 transition, which is the strongest $2s^2\ 2p^2\ 3s$ transition from the ground level and has a level label of $^4P_{5/2}$. Included in the figure are the results from the 3*l* calculation (dot), the 4*l* calculation (solid), Butler & Zeippen (2001) (dot-dash), and Landi & Gu (2006) (dash). At high temperatures, we see very good agreement between the present calculations and those of Landi & Gu. However, due to the error apparent in Fig. 3, the Butler & Zeippen results are too large by more than a factor of two. At low temperatures, all of the calculations disagree due to differences in the resonance structure.

The strongest $2s^2\ 2p^2$ 3p transition has a level label of $^4S_{3/2}$. The effective collision strength for this transition (1−33) is plotted in Fig. 6 where, again, we see very good agreement with the present calculations and those of Landi & Gu at high temperatures. As there is very good agreement between the backgrounds of all the calculations, the discrepancy at low temperatures must be due to resonances. The Landi & Gu results show little resonant enhancement while there is an increasing effect for the 3*l* and 4*l* results, respectively.

As the transitions to the $2s^2\ 2p^2$ 3d levels have little resonant enhancement, the agreement between the present calculations and those of Landi & Gu is good at all temperatures. Shown in Fig. 7 is the transition to the $2s^2\ 2p^2\ 3d\ ^4P_{5/2}$ level (1−56), where we see that the Landi & Gu results are slightly higher than the

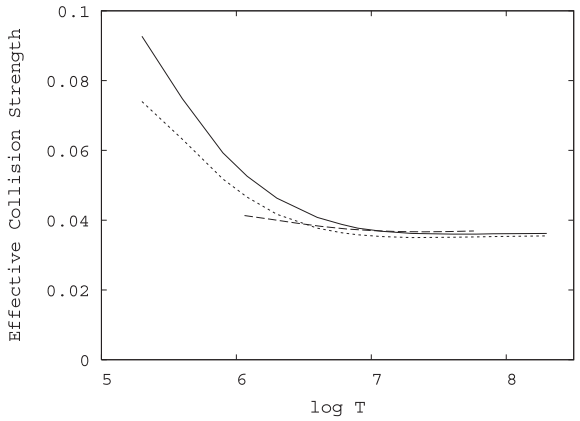

Fig. 6. Effective collision strength for the transition to $2s^2\ 2p^2\ 3p\ ^4S_{3/2}$ from the ground level (1−33). The solid and dotted curves are the $4l$ and $3l$ calculations, respectively, and the dashed curve is the result from Landi & Gu (2006).

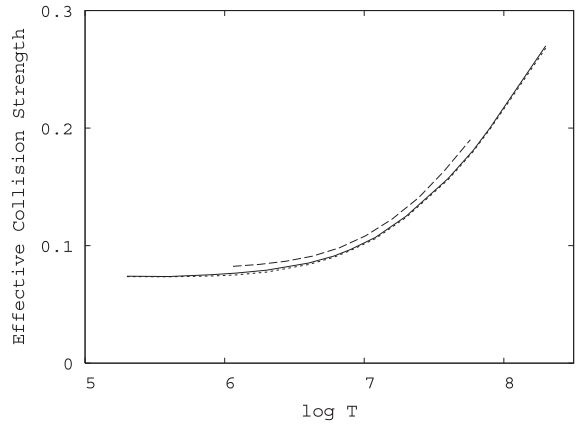

Fig. 7. Effective collision strength for the transition to $2s^2\ 2p^2\ 3d\ ^4P_{5/2}$ from the ground level (1−56). The curve identifications are the same as in Fig. 6.

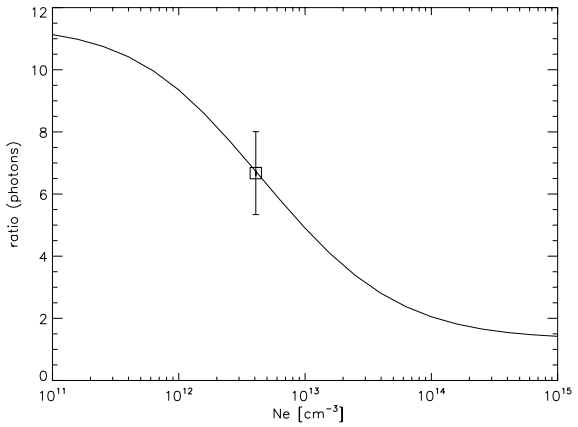

Fig. 8. Theoretical ratio of the 1−56 $^4S_{3/2}$–$^4P_{5/2}$ (12.845 Å) vs. 2−64 $^2D_{3/2}$–$^2D_{5/2}$ as a function of electron density, calculated at $T = 10^7$ K. The box is the measurement of Landi & Phillips (2005).

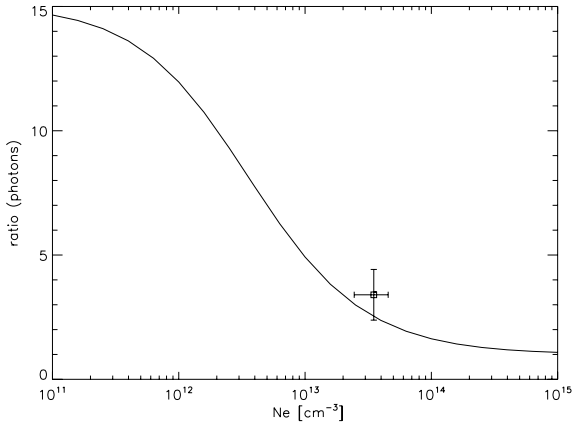

Fig. 9. Theoretical ratio of the $^4S_{3/2}$–$^4P_{3/2}$ (121.845 Å) vs. the $^2D_{3/2}$–$^2D_{3/2}$ (110.627 Å) as a function of electron density, calculated at $T = 10^7$ K. The box is the measurement of Stratton et al. (1984), with 30% error bars.

present calculations (which are in excellent agreement with each other) over the entire temperature range.

Finally, we examine the 1−61 transition, which is also identified in Fig. 4, where level 61 is labeled as $2s^2\ 2p^2\ 3d\ ^2F_{7/2}$ in all the calculations. This transition stands out as it is the only one where the results of Landi & Gu (2006) are significantly larger than for the present calculations. After a discussion with Landi (2006), it was found that a mistake was made in the 1−61 collision strength of the Landi & Gu results where the background collision strength of a dipole transition was accidentally combined with that of the 1−61 transition. Furthermore, Landi points out that this isolated mistake might explain a discrepancy found in Landi & Phillips (2006) for the Fe XX line at 13.091 Å where the predicted emissivity was larger than the observation (from SMM/FCS).

3.2. Transition probabilities and line intensities

We have calculated level populations with the $4l$ dataset assuming steady-state conditions at a temperature where Fe^{19+} has peak abundance in collisional-ionization equilibrium ($T \approx 10^7$ K). We have selected only the brightest transitions in the low-density regime (10^{12} cm^{-3}), applicable to most astrophysical plasmas and low-density laboratory plasmas such as tokamaks. The results are shown in Table 5, where we have compared our transition probabilities with those in the NIST (v. 3) compilation, those calculated by Jonauskas et al. (2005), and within the IRON Project report of Nahar (2004). The A-values of Jonauskas et al. (2005) were calculated using a relativistic structure code, GRASP, and included the lowest 700 levels (up to $n = 5$) in the multi-configuration Dirac-Fock (MCDF) approach. Nahar (2004) used the Breit-Pauli R-matrix (BPRM) codes (Berrington et al. 1995) to calculate the dipole-allowed transitions and SUPERSTRUCTURE (Eissner et al. 1974) for the forbidden transitions, where a correction to observed energies was also included. We find there is excellent agreement (within 10%) of our results with the NIST and Jonauskas et al. (2005) values. Finer refinements (such as the use of observed energies) are still possible, but would only change our results slightly. We therefore recommend, for consistency, that our A-values are used together with our collision rates. On the other hand, we find significant discrepancies with the BPRM values of Nahar (2004)[2]. For the strongest transitions, listed in Table 5, the differences are within a factor of two, however, for weaker transitions differences are

[2] It appears that these large differences are due to a dipole phase error which is present in all versions of the Breit-Pauli R-matrix code, and which has now been corrected (Berrington & Storey 2007). The corrected code can be found at
`http://amdpp.phys.strath.ac.uk/tamoc/code.html`

Table 5. List of all the most prominent lines in Fe^{19+}. Columns 3–5 indicate the theoretical line intensities (photons) calculated with the present $4l$ dataset, the dataset of Landi & Gu (L05), and that of Butler & Zeippen (BZ01). The intensities have been calculated assuming steady-state conditions, in the low density regime (10^{12} cm^{-3}) at $T = 10^7$ K, and are normalised to the intensity of the strongest transition. Columns 6–9 give, respectively, our A-values, those in the NIST database (v. 3), those in Jonauskas et al. (2005 – J05) and in Nahar (2004 – N04). Notable differences are marked with asterisks.

i-j	Terms	I	I(L05)	I(BZ01)	A_{ji}	A_{ji}(NIST)	A_{ji}(J05)	A_{ji}(N04)
				$2s^2\ 2p^3$–$2s^2\ 2p^3$				
1-2	$^4S_{3/2}$–$^2D_{3/2}$	7.3	6.8	6.3	1.6×10^4	–	1.6×10^4	1.4×10^4
1-3	$^4S_{3/2}$–$^2D_{5/2}$	2.8	2.9	2.6	1.3×10^3	1.3×10^3	1.2×10^3	1.1×10^3
1-4	$^4S_{3/2}$–$^2P_{1/2}$	1.2	1.2	1.1	3.3×10^4	–	3.1×10^4	3.0×10^4
1-5	$^4S_{3/2}$–$^2P_{3/2}$	0.69	0.62	0.61	3.1×10^4	2.9×10^4	3.0×10^4	2.9×10^4
2-5	$^2D_{3/2}$–$^2P_{3/2}$	1.0	0.91	0.87	4.6×10^4	4.5×10^4	4.3×10^4	4.3×10^4
2-3	$^2D_{3/2}$–$^2D_{5/2}$	1.2	1.1	0.89	5.8×10^2	2.9×10^4	4.3×10^2	4.2×10^2
3-5	$^2D_{5/2}$–$^2P_{3/2}$	0.26	0.26	0.24	1.2×10^4	–	1.2×10^4	1.2×10^4
2-4	$^2D_{3/2}$–$^2P_{1/2}$	0.22	0.23	0.21	6.0×10^3	–	5.9×10^3	6.1×10^3
				$2s^2\ 2p^3$–$2s^2\ 2p^2\ 3d$				
1-58	$^4S_{3/2}$–$^4P_{3/2}$	1.0	1.1	0.95	2.0×10^{13}	2.1×10^{13}	2.05×10^{13}	1.4×10^{13} *
1-56	$^4S_{3/2}$–$^4P_{5/2}$	0.90	0.95	0.82	1.3×10^{13}	–	1.3×10^{13}	1.3×10^{13}
1-60	$^4S_{3/2}$–$^4P_{1/2}$	0.43	0.45	0.41	1.9×10^{13}	–	1.8×10^{13}	–
1-48	$^4S_{3/2}$–$^4D_{5/2}$	0.29	0.29	0.26	3.4×10^{12}	–	3.1×10^{12}	–
1-52	$^4S_{3/2}$–$^2F_{5/2}$	0.25	0.28	0.22	4.9×10^{12}	–	5.1×10^{12}	–
1-42	$^4S_{3/2}$–$^4F_{5/2}$	0.23	0.25	0.21	2.6×10^{12}	–	2.7×10^{12}	
2-52	$^2D_{3/2}$–$^2F_{5/2}$	0.15	–	0.14	3.0×10^{12}	–	2.7×10^{12}	–
3-61	$^2D_{5/2}$–$^2F_{7/2}$	6.4×10^{-2}	0.53 *	4.9×10^{-2} *	6.8×10^{12}	–	7.0×10^{12}	
				$2s^2\ 2p^3$–$2s^2\ 2p^2\ 3s$				
1-19	$^4S_{3/2}$–$^4P_{5/2}$	0.16	0.21 *	0.36 *	1.1×10^{12}	–	1.1×10^{12}	1.2×10^{12}
1-17	$^4S_{3/2}$–$^4P_{3/2}$	9.8×10^{-2}	0.11	0.22 *	1.1×10^{12}	–	1.1×10^{12}	–
1-16	$^4S_{3/2}$–$^4P_{1/2}$	6.9×10^{-2}	8.5×10^{-2}	0.13 *	1.3×10^{12}	–	1.3×10^{12}	3.6×10^{11} *
3-19	$^2D_{5/2}$–$^4P_{5/2}$	4.0×10^{-2}	5.4×10^{-2}	9.7×10^{-2} *	2.8×10^{11}	–	2.8×10^{11}	2.8×10^{11}
				$2s^2\ 2p^3$–$2s\ 2p^4$				
1-6	$^4S_{3/2}$–$^4P_{5/2}$	15.	15.	14.	1.2×10^{10}	1.3×10^{10}	1.2×10^{10}	1.2×10^{10}
1-7	$^4S_{3/2}$–$^4P_{3/2}$	11.	11.	10.	1.8×10^{10}	1.9×10^{10}	1.7×10^{10}	1.37×10^{10} *
1-8	$^4S_{3/2}$–$^4P_{1/2}$	5.4	5.4	5.2	2.0×10^{10}	2.1×10^{10}	1.9×10^{10}	1.3×10^{10} *
3-12	$^2D_{5/2}$–$^2P_{3/2}$	1.3	1.2	1.2	9.8×10^{10}	1.0×10^{11}	9.7×10^{10}	9.3×10^{10}
3-10	$^2D_{5/2}$–$^2D_{5/2}$	1.1	1.0	0.81	3.1×10^{10}	3.3×10^{10}	3.0×10^{10}	2.9×10^{10}
2-9	$^2D_{3/2}$–$^2D_{3/2}$	0.89	0.70 *	0.64 *	4.1×10^{10}	4.3×10^{10}	4.0×10^{10}	2.5×10^{10} *
2-6	$^2D_{3/2}$–$^4P_{5/2}$	0.65	0.64	0.63	5.5×10^8	–	5.2×10^8	5.2×10^8
2-11	$^2D_{3/2}$–$^2S_{1/2}$	0.22	0.17 *	0.15 *	4.4×10^{10}	4.5×10^{10}	4.3×10^{10}	3.4×10^{10} *
2-12	$^2D_{3/2}$–$^2P_{3/2}$	0.19	0.18	0.17	1.4×10^{10}	1.5×10^{10}	1.5×10^{10}	1.4×10^{10}
5-13	$^2P_{3/2}$–$^2P_{1/2}$	0.16	7.8×10^{-2} *	8.0×10^{-2} *	9.3×10^{10}	9.6×10^{10}	8.3×10^{10}	–
4-11	$^2P_{1/2}$–$^2S_{1/2}$	0.18	0.14 *	0.12 *	3.6×10^{10}	3.7×10^{10}	3.6×10^{10}	3.4×10^{10}
3-6	$^2D_{5/2}$–$^4P_{5/2}$	0.29	0.28	0.28	2.4×10^8	–	2.2×10^8	2.4×10^8
5-10	$^2P_{3/2}$–$^2D_{5/2}$	0.20	0.19	0.15	5.8×10^9	6.0×10^9	5.6×10^9	5.4×10^9
4-12	$^2P_{1/2}$–$^2P_{3/2}$	0.12	0.11	0.10	8.9×10^9	9.1×10^9	8.6×10^9	8.4×10^9
5-12	$^2P_{3/2}$–$^2P_{3/2}$	0.13	0.12	0.11	9.5×10^9	9.4×10^9	9.4×10^9	1.1×10^{10}
				$2s\ 2p^4$–$2p^5$				
10-14	$^2D_{5/2}$–$^2P_{3/2}$	0.12	1.2×10^{-2} *	7.1×10^{-3} *	4.1×10^{10}	4.3×10^{10}	4.1×10^{10}	3.9×10^{10}

much larger as already shown in Table 6 of Nahar (2004). These differences are noted and discussed by Jonauskas et al. (2005).

A second important step in our assessment of the data concerns the line intensities. Not only are we interested in assessing the effects of the additional $n = 4$ levels on the level balance for this ion, but wanted to compare our results (as a complete data set) with other calculations, namely Butler & Zeippen (2001) and Landi & Gu (2006). In Table 5, we list our (normalized) line intensities, compared with those obtained with the Landi & Gu and the Butler & Zeippen datasets, as included in CHIANTI v. 5 and 4 respectively (with the exclusion of ionization/recombination corrections and the inclusion of proton excitations within the ground configuration). It turns out that, at the peak temperature, the results of Landi & Gu are very close to ours (within 10%) with few exceptions (for example, the transition from level 61 where we noted large disagreement in the effective collision strength). Larger discrepancies with the Landi & Gu results are found at higher densities and lower temperatures.

We find that larger differences are found with the Butler & Zeippen data overall, but, in most cases, still within 20%. Significant exceptions listed in Table 5 are clearly due to the erroneous "jumps" of the high energy collision strenths in the Butler & Zeippen calculation. Finally, in contrast to our previous work on Fe^{17+} (Witthoeft et al. 2006), we have found that the inclusion of the $n = 4$ levels did not significantly affect the line intensities for this ion at the peak abundance temperature for collisionally-ionized plasmas.

A complete benchmark on identifications, observed wavelengths and diagnostic possibilities for astrophysical and laboratory plasmas is beyond the scope of this paper, however, a few comments are worth mentioning here. The forbidden transitions within the $2s^2\ 2p^3$ ground configurations are strong in solar flares, as shown in Kucera et al. (2000). As the same authors point out, these lines can potentially be very useful in the cross-calibration of instruments observing the 300−2700 Å spectral range (as long as densities are below 10^{11}). The $2s^2\ 2p^3$–$2s^2\ 2p^2\ 3d$ transitions are prominent in the X-ray spectra of solar flares and active stars. One particular strong transition, 2−64 ($^2D_{3/2}$–$^2D_{5/2}$), is an useful density diagnostic when observed in conjunction with one of the other transitions to the ground state. Fig. 8 shows one example, with the measurement from an SMM spectrum of a solar flare (Landi & Phillips 2005). In this particular case, an electron density of approximately $10^{12.6}$ cm^{-3} is obtained.

The $2s^2\ 2p^3$–$2s\ 2p^4$ lines are also prominent in solar flares, however most of them are blended with lines from other ions. Notably, the 1−6 line with the resonance of Fe^{22+}. As already found by previous authors (see, e.g. Stratton et al. 1984), the 1−7 (121.845 Å) and 2−9 (110.627 Å) lines are notable exceptions, and their ratio is an excellent density diagnostic. Figure 9 shows that our results are in close agreement (30%) with the measurements of Stratton et al. (1984).

4. Summary

Two ICFT *R*-matrix calculations were performed for the electron-impact excitation of Fe^{19+}. This work expands upon, and corrects an error in, the previous IRON Project work by Butler & Zeippen (2001). Effective collision strengths for all 45 451 transitions of the larger calculation have been archived. We find excellent agreement of our collision strengths with the recent work of Landi & Gu (2006) at high temperatures, but there are significant differences at lower temperatures where resonant enhancement plays a larger role. We find little difference in level populations between our results and the work of Landi & Gu for a low density N-like Fe plasma at 10^7 K, however, at lower temperatures (for photo-ionized plasmas), we recommend using the present 4*l* dataset due to the more accurate treatment of resonance contributions. We have noted large differences of some A-values with those from a previous IRON Project report (Nahar 2004), but we are confident in the soundness of the present A-values from comparisons with both NIST and the calculation of Jonauskas et al. (2005). In conclusion, we have provided a robust and complete set of collision strengths and transition probabilities up to $n = 4$ to be used for astrophysical and laboratory plasma applications.

Acknowledgements. This work has been funded by PPARC grant PPA/G/S2003/00055. GDZ acknowledges support from PPARC and warmly thanks DAMTP, University of Cambridge for the hospitality. We would also like to thank Enrico Landi for his input.

References

Badnell, N. R. 1986, J. Phys. B: At. Mol. Phys. 19, 3827
Badnell, N. R., & Griffin, D. C. 2001, J. Phys. B: At. Mol. Opt. Phys. 34, 681
Berrington, K. A., & Storey, P. J. 2007, private communication
Burgess, A. 1974, J. Phys. B: At. Mol. Phys., 7, L364
Butler, K. 2006, private communication
Butler, K., & Zeippen, C. J. 2001, A&A, 372, 1078
CHIANTI web page: `http://www.chianti.rl.ac.uk`
Eissner, W., Jones, M., & Nussbaumer, H. 1974, Comp. Phys. Comm., 8, 270
Griffin, D. C., Badnell, N. R., & Pindzola, M. S. 1998, J. Phys. B: At. Mol. Opt. Phys., 31, 3713
Gu, M. F. 2003, ApJ, 582, 1241
Hummer, D. G., Berrington, K. A., Eissner, W., et al. 1993, A&A, 279, 298
Jonauskas, V., Bogdanovich, P., Keenan, F. P., et al. 2005, A&A, 433, 745
Kallman, T., & Bautista, M. 2001, ApJS, 133, 221
Kastner, S. O., Neupert, W. M., & Swartz, M. 1974, ApJ, 191, 261
Kucera, T. A., Feldman, U., Widing, K. G., & Curdt, W. 2000, ApJ, 538, 424
Landi, E. 2006, private communication
Landi, E., & Gu, M. F. 2006, ApJ, 640, 1171
Landi, E., & Phillips, K. J. H. 2006, ApJS, 166, 421
Landi, E., Del Zanna, G., Young, P. R., et al. 2006, ApJS, 162, 261
Mason, H. E., & Bhatia, A. K. 1983, A&AS, 52, 181
Mazzotta, P., Mazzitelli, G., Colafrancesco, S., & Vittorio, N. 1998, A&AS, 133, 403
McLaughlin, B. M., & Kirby, K. P. 2001, J. Phys. B: At. Mol. Opt. Phys., 34, 2255
Nahar, S. N. 2004, A&A, 413, 779
NIST web page: `http://physics.nist.gov/PhysRefData/ASD/`
Stratton, B. C., Moos, H. W., & Finkenthal, M. 1984, ApJ, 279, L31
Whiteford, A. D., Badnell, N. R., Ballance, C. P., et al. 2001, J. Phys. B: At. Mol. Opt. Phys., 34, 3179
Witthoeft, M. C., Badnell, N. R., Del Zanna, G., Berrington, K. A. & Pelan, J. C. 2006, A&A, 446, 361